Tennessee Valley Authority, 1101 Market Street, LP 5A, Chattanooga, Tennessee 37402-2801

October 20, 2008

10 CFR 52.79

U.S. Nuclear Regulatory Commission
ATTN: Document Control Desk
Washington, D.C. 20555

In the Matter of)
Tennessee Valley Authority)

Docket No. 52-014 and 52-015

BELLEFONTE COMBINED LICENSE APPLICATION – RESPONSE TO REQUEST FOR ADDITIONAL INFORMATION – VIBRATORY GROUND MOTION

Reference: Letter from Joseph Sebrosky (NRC) to Andrea L. Sterdis (TVA), Request for Additional Information Letter No. 125 Related to SRP Section 2.5.2 for the Bellefonte Units 3 and 4 Combined License Application, dated September 19, 2008

This letter provides the Tennessee Valley Authority's (TVA) response to the Nuclear Regulatory Commission's (NRC) request for additional information (RAI) items included in the reference letter.

A response to each NRC request in the subject letter is addressed in the enclosure which does not identify any associated changes to be made in a future revision of the BLN application.

If you should have any questions, please contact Thomas Spink at 1101 Market Street, LP5A, Chattanooga, Tennessee 37402-2801, by telephone at (423) 751-7062 or via email at tespink@tva.gov.

I declare under penalty of perjury that the foregoing is true and correct.

Executed on this 20th day of Oct, 2008.

Andrea L. Sterdis
Manager, New Nuclear Licensing and Industry Affairs
Nuclear Generation Development & Construction

Enclosure
cc: See Page 2

D085
NRO

cc: (w/ Enclosures)
J. P. Berger, EDF
J. M. Sebrosky, NRC/HQ
E. Cummins, Westinghouse
S. P. Frantz, Morgan Lewis
M. W. Gettler, FP&L
R. Grumbir, NuStart
P. S. Hastings, NuStart
P. Hinnenkamp, Entergy
M. C. Kray, NuStart
D. Lindgren, Westinghouse
G. D. Miller, PG&N
M. C. Nolan, Duke Energy
N. T. Simms, Duke Energy
K. N. Slays, NuStart
G. A. Zinke, NuStart

cc: (w/o Enclosure)
B. C. Anderson, NRC/HQ
M. M. Comar, NRC/HQ
B. Hughes/NRC/HQ
R. G. Joshi, NRC/HQ
R. H. Kitchen, PGN
M. C. Kray, NuStart
A. M. Monroe, SCE&G
C. R. Pierce, SNC
R. Reister, DOE/PM
L. Reyes, NRC/RII
T. Simms, NRC/HQ

Enclosure
TVA letter dated October 20, 2008
RAI Response

Response to NRC Request for Additional Information letter No. 125 dated September 19, 2008
(20 pages, including this list)

Subject: Vibratory Ground Motion in the Final Safety Analysis Report

RAI Number	Date of TVA Response
02.05.02-02	This letter – see following pages
02.05.02-03	This letter – see following pages
02.05.02-04	This letter – see following pages
02.05.02-05	This letter – see following pages
02.05.02-06	This letter – see following pages
02.05.02-07	This letter – see following pages
02.05.02-08	This letter – see following pages

Associated Additional Attachments / Enclosures	Pages Included
Attachment 02.05.02-02A	2
Attachment 02.05.02-02B	2
Attachment 02.05.02-02C	2
Attachment 02.05.02-02D	2
Attachment 02.05.02-02E	2
Attachment 02.05.02-03A	2
Attachment 02.05.02-03B	2
Attachment 02.05.02-03C	5
Attachment 02.05.02-04A	2

NRC Letter Dated: September 19, 2008

NRC Review of Final Safety Analysis Report

NRC RAI NUMBER: 02.05.02-02

FSAR Section 2.5.2.5 describes the site as a hard rock site and states that two thirds of the measured rock section exhibits shear wave velocity of 9,200 fps or greater. Please explain whether the existence of the layer C disqualifies the site as a "hard rock" site because the layer has a shear wave velocity of about 6000 fps (FSAR Figure 2.5.-299) and provide the basis for your decision not to do a site response analysis to evaluate the effect of the underlying lower shear wave velocity layer. In addition, please explain the potential impact of this material on the GMRS calculation.

BLN RAI ID: 1832

BLN RESPONSE:

Two definitions of "hard rock" are used for this RAI response; 1) the AP-1000 Design Control Document (DCD) design soil profile definition presented in DCD Subsection 3.7.1.4 "Supporting Media for Seismic Category I Structures", and 2) the Electric Power Research Institute (EPRI; 2004, 1993) (References 5 and 13) (FSAR Subsection 2.5.7, References 350 and 451) definition used for application of central-eastern U.S. (CEUS) attenuation models for site response analyses.

Figure 1 (Attachment 02.05.02-02A) shows that layer C comprises about 20% of the surface footprint of Bellefonte Reactor Unit 3. After accounting for interface depth and dip uncertainties, the maximum thickness of layer C beneath Reactor Unit 3 of about 16 ft occurs in the southeast corner of the Reactor Unit 3 footprint. The portion of layer C beneath the Reactor Unit 3 footprint corresponds to the bottom <16 ft of layer C in the stratigraphic section as shown on Figure 2 (Attachment 02.05.02-02B). Figure 2 also shows that three velocity logs intersect this lowest 16 ft section of layer 3. As shown on Figure 3 (Attachment 02.05.02-02C), these velocity logs demonstrate that a conservative estimate of the average shear-wave velocity of layer C beneath Reactor Unit 3 is 7000 ft/s. The closest portion of layer C to the Reactor Unit 4 footprint is 110 ft below plant grade (Figure 2).

With respect to DCD criteria, five soil profiles are used to envelope sites where the shear wave velocity of the supporting medium at foundation level exceeds 1,000 feet per second (ft/sec); hard rock, firm rock, upper bound soft-to-medium soil, soft-to-medium soil, and soft soil. The upper bound case for hard rock is defined at shear-wave velocity of 8,000 ft/sec. Firm rock is defined at a shear-wave velocity of 3,500 ft/sec. The average shear-wave velocity for layer C of 7,000 ft/sec, described above, falls between the DCD criteria for upper bound hard rock and firm rock, and therefore correlates with a hard rock enveloping condition. Therefore, the foundation media supporting the nuclear islands of both Units 3 and 4 at basemat elevation qualify as hard rock supporting media using the DCD criteria. This includes the portions of the footprints underlain by the layer C material. Detailed discussion of the foundation properties and the DCD criteria is provided in the response to NRC RAI NUMBER: 02.05.04-05, which demonstrates that the foundation satisfies both the AP1000 DCD Subsections 2.5.4.5 and 2.5.4.5.3 requirements to classify a site as "uniform" and required limits on lateral variability.

With respect to the EPRI criteria, the departure of site-specific shear-wave velocities from that of the reference hard rock site condition cited in EPRI (2004, 1993) (Reference 5, 13) of a uniform 2.84 km/sec (9,318 ft/sec) over the top kilometer of a site is both expected at actual sites as well as accommodated in the hard rock hazard analysis. In terms of consistency with the EPRI (2004) (Reference 5) attenuation relations, the issue centers on both the appropriate range in overall shear-wave velocities averaged over depth (e.g. 10m to 50m) at hard rock sites in central and eastern North America (including basement material beneath soil sites) as well as velocity fluctuations with depth. The velocity fluctuations with

depth include both random and deterministic (relatively soft or stiff zones) fluctuations that occur within all rock sites due to vertical and lateral heterogeneities. Vertical length scales typically range from less than a meter, resolvable only by suspension log surveys with frequencies 0.5 k Hz to 1.0 k Hz, to meters. It is likely such fluctuations represent a considerable contribution to the observed loss in high frequency energy observed at hard rock sites due to scattering over the top 1 to 2 km and parameterized through kappa (Anderson and Hough, 1984) (Reference 1). For hard rock sites in the CEUS, defined broadly as granitic plutons, carbonates, or shield regions, kappa values range from about 0.004 sec to 0.016 sec (Silva and Darragh, 1995) (Reference 9). This range is likely due to the degree of fracturing and heterogeneity and reflected in the range in overall shear-wave velocities as well as velocity gradients with depth.

At rock sites, the net amplification is controlled by two factors: the velocity gradient, which gives rise to amplification as the wavefield propagates from the source to the site; and kappa, which decreases amplitudes through hysteretic damping (Reference 13). The two factors are strongly related to rock quality (e.g., geology) (Reference 9) and both are reflected in ranges of values for hard rock site conditions. Because kappa is difficult to measure in the absence of recorded ground motions, shear-wave velocity has by default been taken as a single parameter or measure of site condition for quantifying strong ground motions. Because site amplification (neglecting energy loss due to damping) depends strongly on frequency, with shallow velocities controlling the higher frequencies, a velocity average (more accurately travel time) over depth has been accepted as a means of quantifying amplification of strong ground motions over a wide frequency range. The average shear-wave velocity over the top 30 m, $\overline{V_S}$ (30m), has been shown to provide a stable and distinguishing estimate of strong ground motion amplitude at both soil and soft to firm rock sites for $\overline{V_S}$ (30m) ranging from about 180 m/sec to about 900 m/sec in Western North America (WNA) (e.g., NGA, 2008)(Reference 12). The depth of 30 m was adopted largely through necessity as most boreholes at or near strong motion sites typically extend to depths of about 25m to 30 m. Fortunately, in tectonically active regions, the velocities gradient captured over the top 30m is a reliable predictor of the deeper velocities and thereby provides a reasonably robust predictor of low-frequency motions (e.g. $\leq$ 1 Hz). In other words, $\overline{V_S}$ (30m) is correlated with depth to basement material in tectonically active regions (NGA, 2008). In terms of a predictor for strong ground motions, it is important to point out that for very stiff sites (firm rock with $\overline{V_S}$ (30m) > 1,500 m/sec) the uncertainty (epistemic) in $\overline{V_S}$ (30m) is about 0.3 ($\sigma_{\mu \ln}$) and is reflected in the aleatory variability about the NGA WNA relation (Reference 12).

For hard rock environments, either in WNA (Reference 9) or Central and Eastern North America (CENA), it is reasonable to assume that the more robust characterization of strong ground motions in terms of a single site parameter would involve an average over depth, rather than a single value near or at the surface. Additionally, as in WNA, in the development of either empirical or model driven hard rock ground motion models in the CENA, a range in hard rock velocities are accommodated in the aleatory variabilities about each model median as well as epistemic uncertainty between median estimates.

Implicit in the EPRI (2004) (Reference 5) hard rock attenuation relations is a range in both outcrop (and base of soil) shear-wave velocities as well as kappa values. The single value of 2.84 km/sec for hard rock site conditions was based on the EPRI (1993) (Reference 13) crustal regionalization taken from the compressional-wave models in the monograph of Pakiser and Mooney (1989) (Reference 7). In the EPRI (1993) (Reference 13) work, some 8 to 10 crustal models were used in simulations to examine potential differences in predictions of strong ground motions. In the modeling effort, since only compressional-wave crustal models were available, shear-wave values were developed by assuming a Poisson ratio of 0.25. Additionally, since many of the crustal models lacked a shallow ($\approx$ 1 km) layer, the top layer of the

Midcontinent crustal model (Reference 7) was adopted for several regions. In the EPRI (1993) (Reference 13) analyses, only two crustal regions reflected a stable and significant difference in wave propagation characteristics, the Gulf Coastal Region and everything else. The Midcontinent crustal model was selected to represent the entire CENA hard rock site condition, apart from the Gulf Coastal Region, as it resulted in expected motions similar to those predicted using the remaining models. The lowest shear-wave velocity considered in the EPRI (1993) (Reference 13) analysis was the Northern Grenville-Superior region with a velocity of 2.34 km/sec over the top 1 km and with the greatest velocity being that of the Midcontinent crustal model at 2.83 km/sec. EPRI (1993) (Reference 13) also considered the effects of a range in Poisson ratio on the shallow shear-wave velocities resulting in shear-wave velocities for the top layer of the Midcontinent crustal model varying from 2.59 km/sec to 2.95 km/sec. Since this range was within that of the crustal models analyzed, the effects of uncertainty in Poisson ratio was considered to have been accommodated in the regionalization. As a result of the EPRI (1993) (Reference 13) analyses, the range in hard rock shear-wave velocities over the top kilometer or so of the crust is from about 2.60 km/sec to 2.95 km/sec. This range in shallow crustal shear-wave velocities is accommodated in terms of wave propagation by a velocity of 2.83 km/sec.

In terms of the EPRI (2004) (Reference 5) attenuation relations, both the aleatory and epistemic variabilities accounted for in the numerical, empirical, and semi-empirical models likely accommodate an even wider range in overall shallow crustal velocities as well as velocity fluctuations. To consider the numerical models, two models which reflect the most complete treatment of parametric variability and corresponding aleatory variability in expected motions were those by Toro et al. (1997) (Reference 11) and Silva (EPRI, 2004) (Reference 5). In those models, the top 30m of the crustal model was randomized using a profile randomization scheme which accommodates a distribution of velocities at depth as well as correlation of velocities with depth, both based on an analysis of variance of over 500 measured shear-wave velocity profiles (Reference 13 and Reference 8). Randomized profiles, about a base-case profile, here a uniform 2.83 km/sec, can then have realistic high and low velocity fluctuations with depth as well as high and low overall or mean average velocities (e.g. $\overline{V_S}$ (30m)). An example of the median and $\pm 1\sigma$ velocity profiles is shown in Attachment 02.05.02-02D - Figure 4 based on 100 realizations. As Figure 4 (Attachment 02.05.02-02D) shows, the $\pm 1\sigma$ range is about 2 km/sec to 4 km/sec and is accommodated in the high frequency aleatory variability about the median attenuations relation. This is not to say that the entire range in $\pm 1\sigma$ profiles over 30m or more is accommodated in the aleatory variability but does demonstrate fluctuations at the surface or with depth as low as 2 km/sec and of several meters extent are realistic for a hard rock site.. This is demonstrated in the suspension log results at the two hard rock wells drilled in the hard rock granite near the Monticello Reservoir in South Carolina (Moos and Zoback, 1983) (Reference 6). The two well logs (Figures 4, 5; Moos and Zoback, 1983)(Reference 6) show average shear-wave velocities near 3 km/sec over the top approximately 900m (logs beginning at a depth of about 50m) with numerous fluctuations to velocities of 2.5 km/sec and lower. A steep velocity gradient is also seen over the shallow portion of the logs suggesting a near surface velocity of about 2.5 km/sec.

For the empirical wave propagation ground motion models in EPRI (2004) (Reference 5) (e.g., Atkinson and Boore 1997)(Reference 2), a shallow shear-wave refraction survey of several seismographic sites in eastern Canada (Beresnev and Atkinson, 1997) (Reference 3) shows shallow hard rock velocities ranging from about 2.1 km/sec to about 3.1 km/sec. Based on these surveys, the authors concluded the average shear-wave velocity for hard rock sites reflecting the Atkinson and Boore (1997) (Reference 2) attenuation relation is about 2.6 km/sec. Based on their interpretations of the refraction surveys, these hard rock shear-wave velocities reflect averages over at least 20m to 40m. Note that the lower range shear-wave velocity of 2.1 km/sec (6,888 ft/sec) measured at the eastern Canada sites is essentially the same as the measured lowest shear-wave velocity in the lower 16 ft of layer C at the Bellefonte site (Attachment 02.05.02-02C – Figure 3).

Considering finally the semi-empirical ground motion relation in EPRI (2004) (Reference 5), Campbell (2003) (Reference 4) began with his western North America (WNA) rock relation and used transfer functions to adjust it to CENA conditions. Implicit in the aleatory variability of this relation is the component due to the range in average shear-wave velocities as well as velocity fluctuations with depth in

the rock sites included in the WNA relation. To illustrate this range of shear-wave velocities, Figure 5 (Attachment 02.05.02-02E) shows the median and $\pm$ 1σ profile at recording sites classified as rock (Geomatrix categories A and B) in tectonically active regions (e.g., WNA). While the CENA and WNA profiles appear quite different, the overall σ_{ln} (lognormal standard deviations) are similar, about 0.6 to 0.7. This observation suggests the aleatory variability in the semi-empirical model incorporated in the EPRI (2004) (Reference 5) ground motion relations incorporates a range in velocity profiles as well as velocity fluctuations with depth.

To summarize, the stated hard rock shear-wave velocity of 2.84 km/sec in EPRI (2004, 1993) reflects the shear-wave velocity representative of the top 1 km of the Midcontinent crustal model. Except for the Gulf Coastal region, based on numerical simulations (EPRI, 1993) (Reference 13), this model reflects the expected wave propagation effects from the remaining CENA crustal models with shear-wave velocities ranging from 2.34 km/sec to 2.95 km/sec over the top 1 km or so. Results of shallow shear-wave refraction surveys in eastern Canada suggest hard rock near surface velocities average about 2.6 km/sec and range from about 2.1 km/sec to about 3.1 km/sec. These observations do not represent an entire kilometer of crust but are more representative of averages over 20m to 40m. Further examination of suspension log shear-wave velocities at a hard rock site in South Carolina show average velocities over the top appropriately 800m of about 3 km/sec with fluctuations with depth over a significant vertical extent to about 2.5 km/sec and somewhat lower. Both the fluctuations in velocity with depth and the ranges in overall or average velocity are accommodated in the EPRI (2004) (Reference 5) ground motion models.

For application to rock layer C beneath the Bellefonte Unit 3 foundation mat, the average shear-wave velocity for layer C beneath the foundation mat is at least 7,000 ft/sec (2.1 km/sec) with a maximum thickness of about 16 ft (Figure 2- Attachment 02.05.02-02B and Figure 3 -Attachment 02.05.02-02C). While the resonant frequency for amplification of Fourier amplitude spectra for the maximum thickness of layer C in contact with the foundation mat is about 110 Hz, the amplification for 5% damped response spectra can propagate to considerably lower oscillator frequency. This arises as the width of oscillator transfer functions increase linearly with oscillator frequency while at high-frequency (> 30 Hz) the Fourier amplitude spectra are rapidly decreasing. As a result the high-frequency oscillators incorporate lower frequency energy potentially resulting in amplification at lower frequency for 5% damped response spectra than Fourier amplitude spectra (Silva et al., 1986) (Reference 10).

Alternatively and more importantly, potential amplification due to laterally continuous surficial or at-depth low-velocity fluctuations has been accommodated in the range of hard rock site conditions incorporated in the EPRI (2004) (Reference 5) strong ground motion relations. As previously discussed, the range in shear-wave velocities over the top kilometer of the crust was as low as 2.34 km/sec for the Midcontinent region (EPRI, 1993) (Reference 13). This velocity of 2.34 km/s is comparable to the average shear-wave velocity of 2.13 km/s (7000 ft/s) measured in the lowest 16 ft of layer C shown in Figure 3 (Attachment 02.05.02-02C). Additionally, for the empirical wave propagation models incorporated in the EPRI (2004) (Reference 5) hard rock relations, a limited shear-wave refraction survey showed shear-wave velocities as low as about 2.1 km/sec averaged over about 40m (Beresnev and Atkinson, 1997) (Reference 3). Below layer C, the shear-wave velocities are about 9,500 ft/sec (approaching about 10,000 ft/sec) giving an average over 100 ft (including the layer C portion) of about 9,000 ft/sec ($\approx$ 2.7 km/sec). This average is well within the range of average hard rock velocities incorporated in the EPRI (2004) (Reference 5) hard rock strong ground motion relations.

Additionally only a small portion of rock layer C intersects less than about 20% of the foundation mat of Unit 3 due to the approximately 17° dip. Such occurrences are reasonably considered to have the same effects as velocity fluctuations which may or may not be laterally continuous, giving rise to spatial incoherency at high frequency. Such variances at rock sites are included in the aleatory variability about the EPRI (2004) (Reference 5) median attenuation relations. At Unit 3, the maximum thickness of 16 ft of approximately 7,500 ft/sec material overlying massive hard rock with shear-wave velocities between

9,500 ft/sec and 10,000 ft/sec is considered to be well within the range of hard rock site conditions incorporated in the EPRI (2004) (Reference 5) ground motion relations. As a result, both the potential amplification, as well as variability attributed to departures from a uniform velocity of 9,200 ft/sec (from Regulatory Guide 1.208, Appendix E), are accommodated in the EPRI (2004) (Reference 5) relations and the site as well as GMRS qualify as a hard rock site.

References:

1) Anderson, J. G. and S. E. Hough (1984). "A Model for the Shape of the Fourier Amplitude Spectrum of Acceleration at High Frequencies." *Bull. Seism. Soc. Am.*, 74(5), 1969-1993.

2) Atkinson, G.M. and Boore, D.M. (1997). "Stochastic point source modeling of ground motions in the Cascadia Region." *Seism. Res. Lett.*, 68(1), 74-90.

3) Beresnev, I.A. and G. M. Atkinson (1997). "Modeling finite-fault radiation from the ω" spectrum." *Bull. Seism. Soc. Am.*, 87(1), 67-84.

4) Campbell, K. W. (2003). "Prediction of strong ground motion using the hybrid empirical method and its use in the development of ground-motion (attenuation) relations in eastern North America." *Bull. Seism. Soc. Am.*, 93(3), 1012-1033.

5) Electric Power Research Institute (2004). "CEUS Ground motion project" Palo Alto, Calif: Electric Power Research Institute, Final Report, EPRI Technical Report 1009684.

6) Moos, D. and M. D. Zoback (1983). "In Situ Studies of Velocity in Fractured Crystalline Rocks." *Journal of Geophysical Research*, 88(B3), 2345-2358.

7) Pakiser, L.C. and W. D. Mooney (1989). "Geophysical Framework of the Continental United States." *Geological Society of America Memoir* 172.

8) Silva, W.J. (1997). "Characteristics of vertical strong ground motions for applications to engineering design." Proc. Of the FHWA/NCEER Workshop on the Nat=l Representation of Seismic Ground Motion for New and Existing Highway Facilities, I.M. Friedland, M.S Power and R. L. Mayes eds., Technical Report NCEER-97-0010.

9) Silva, W.J., and R. Darragh, (1995). "Engineering characterization of earthquake strong ground motion recorded at rock sites." Palo Alto, Calif.: Electric Power Research Institute, Final Report RP 2556 48.

10) Silva, W.J., T. Turcotte and Y. Moriwaki (1986). "Soil response to earthquake ground motions." Palo Alto, Calif.: Electric Power Research Institute, EPRI Research Project RP 2556-07.

11) Toro, G.R., N.A. Abrahamson, and J.F. Schneider (1997). "Model of strong ground motions from earthquakes in Central and Eastern North America: Best estimates and uncertainties." *Seismological Research Lett.*, 68(1), 41-57.

12) NGA (2008). Earthquake Spectra Issue about NGA, *Earthquake Spectra*, 24(1), 1-341.

13) Electric Power Research Institute (1993) "Guidelines for determining design basis ground motions." Palo Alto, Calif: Electric Power Research Institute, vol. 1-5, EPRI TR-102293. Includes:

This response is PLANT SPECIFIC.

ASSOCIATED BLN COL APPLICATION REVISIONS:

No COLA revisions are associated with this response.

ASSOCIATED ATTACHMENTS/ENCLOSURES:

Attachment 02.05.02-02A

Attachment 02.05.02-02B

Attachment 02.05.02-02C

Attachment 02.05.02-02D

Attachment 02.05.02-02E

NRC Letter Dated: September 19, 2008

NRC Review of Final Safety Analysis Report

NRC RAI NUMBER: 02.05.02-03

FSAR Subsection 2.5.2.1.2, "Recent Earthquake and Historical Seismicity" describes basic parameters associated with the April 29, 2003, Fort Payne earthquake. Please explain the uncertainty in determining the focal depth of the earthquake in terms of the distance of the nearest seismography station, seismic network distribution, availability of aftershock network, velocity structures and direct evidence from seismograms. In addition, please provide an explanation on depth uncertainties for the events plotted in the FSAR Figure 2.5-294. Given the level of the uncertainty in determining the depth of an earthquake in the area, please explain how you determined these events related not to ruptures above the detachment (for example, on the Sequatchie fault) but rather to the mid crust structures beneath the detachment.

BLN RAI ID: 1833

BLN RESPONSE:

The information requested in this RAI can be subdivided into three separate issues. The response is organized by each of these issues listed below:

1. Please explain the uncertainty in determining the focal depth of the earthquake in terms of the distance of the nearest seismography station, seismic network distribution, availability of aftershock network, velocity structures and direct evidence from seismograms.
2. Please provide an explanation on depth uncertainties for the events plotted in FSAR Figure 2.5-294.
3. Please explain how you determined these events are not related to ruptures above the detachment (for example, on the Sequatchie fault) but rather to the mid crust structures beneath the detachment.

Issue 1

Several institutions have reported hypocentral locations for the Fort Payne earthquake of 29 April 2003. These institutions include: Virginia Tech Seismological Observatory (FSAR Subsection 2.5.7, Reference 407), Center for Earthquake Research and Information (CERI) (Reference 3), and St. Louis University Earthquake Center (FSAR Subsection 2.5.7, Reference 343). There is considerable variability in the reported depths of the Fort Payne earthquake that largely reflects the different methodologies of and datasets used in estimating the hypocenter. For example, CERI reports a depth of 19.6 km and does not provide any information on the uncertainty (Reference 3). Virginia Tech reports a depth of 9.1 km for the earthquake with a 0.4 km largest-vertical deviation of the 68% confidence ellipsoid from this depth (FSAR Subsection 2.5.7, Reference 407; Reference 4). The Virginia Tech location is shown in FSAR Figure 2.5-294, and the stations used to estimate this location are shown in Figure 1 (Attachment 02.05.02-03A). The closest station to the earthquake was approximately 64 km to the north-northwest. St. Louis University reports a depth of 12 km for the earthquake from a focal mechanism inversion using broadband instrument recordings, and separately a preferred depth of 8 km, estimated using surface wave recordings, though the data can be almost equally as well explained with a depth between approximately 7 km to 17 km (FSAR Subsection 2.5.7, Reference 343).

Additional constraints on the depth of the Fort Payne earthquake come from the distribution of aftershocks following the main earthquake and a regional wave propagation study. Withers et al. (2004) (Reference 5) analyzed aftershocks for several months after the earthquake using a temporary and

regional seismic network. They identified 49 aftershocks, 37 of which were located with the temporary network, and conclude that "aftershock depths were well constrained by the portable network, with most

lying between 12 and 16 km." This observation suggests that the Fort Payne mainshock also occurred near this depth range. In addition, no fault was clearly defined by the aftershock pattern. As part of a separate regional wave-propagation study, Jemberie and Langston (FSAR Subsection 2.5.7, Reference 346) constrained the depth of the earthquake from P and sP arrivals to be between 9.5 and 13 km.

The only formal uncertainty estimate within the studies reviewed above is that from Virginia Tech, and this reported uncertainty is within the range of other depth estimates for the Fort Payne earthquake (7 to 19 km). This considerable range is not surprising given the variety of methods and data sources used to estimate the hypocentral location. Despite this range and uncertainty, the clustering of the depth estimates at 7 km and deeper strongly suggests that the Fort Payne earthquake occurred well within the crystalline basement, which occurs at a depth of approximately 2 to 2.5 km near the earthquake (see FSAR Figure 2.5-220), and not within the overlying Paleozoic sediments.

Issue 2

The earthquakes shown in FSAR Figure 2.5-294 are from the Virginia Tech Seismological Observatory catalog (FSAR Subsection 2.5.7, Reference 407). Most of the events within this catalog have standard error estimates in the form of 68% confidence error ellipsoids derived by the location program Hypoellipse (Reference 2). These ellipsoids show the horizontal and vertical projections of a joint spatial confidence region for the hypocenter under the assumption of normally distributed phase arrival-time reading errors. The reported uncertainties do not take into account bias due to error in the velocity model used to locate the events. Such bias can be significant for focal depth estimates in cases where there are no recording stations within a focal-depth distance of the epicenter. The bias is less significant in the horizontal plane, provided that the event is recorded by at least one station in each azimuthal quadrant surrounding the epicenter. However, the velocity models used for the various hypocenters have generally been developed specifically for the region of the southeastern U.S. including the Bellefonte site (e.g., FSAR Subsection 2.5.7, Reference 292; Reference 6, Bollinger et al., 1979) and are used by most seismograph network operators within the region.

Depths and depth uncertainties for the earthquakes shown in FSAR Figure 2.5-294 are available from the Southeastern United States Seismic Network Bulletins maintained by the Virginia Tech Seismological Observatory (Reference 4) and reproduced in Table 1 (Attachment 02.05.02-03C). The depth uncertainties are reported as the largest vertical deviation of the 68% confidence ellipse from the hypocentral location. Earthquakes that are considered to have well-constrained depths are indicated. Well-constrained earthquakes are defined here as those earthquakes with a 68% confidence vertical error ellipsoid projection of 5 km or less and that were recorded by at least one station within 20 km of the epicenter. Only 19 of the earthquakes are considered to have well constrained depths.

Issue 3

As discussed in FSAR Subsection 2.5.1.1.4.2.4.2, the general scientific consensus regarding seismicity within the Eastern Tennessee Seismic Zone (ETSZ), including the earthquakes shown in FSAR Figure 2.5-294, is that the earthquakes occur below the Alleghanian thrust sheets and associated detachment (see references within FSAR Subsection 2.5.1.1.4.2.4.2 and Reference 1). This conclusion was reevaluated for the Bellefonte COLA project in part using the seismicity data shown in FSAR Figure 2.5-294 and Table 1. This analysis is summarized in response to RAI question 02.05.01-3 (BLN-RAI-LTR-123) provided below. Figures 1 and 2 in Attachment 02.05.01-03A from that response are provided as Attachments 02.05.02-03A and B to this response.

Figure 1 (Attachment 02.05.02-03A) shows the projections of the 68% hypocenter error ellipsoids in the horizontal plane for instrumentally located earthquakes in the site vicinity as reported in Table 1. Most earthquakes within 25 km of the site are located to the northwest of the surface trace of Sequatchie Valley thrust, of Late Paleozoic age, which dips to the southeast. Figure 1 shows that the epicenter semi-major

error ellipse axes (68% confidence) are on the order of 2 km or less for most of these events, suggesting that they are determined with sufficient accuracy to support the interpretation that the majority occurred to the northwest of the Sequatchie Valley fault and therefore, have no relation to that feature.

Earthquakes with computed epicenters to the southeast of the Sequatchie Valley fault trace could be, in principle, associated with that Paleozoic fault, or others to the southeast shown in FSAR Figure 2.5-294. The critical issue in evaluating any potential association between these earthquakes and faults is the focal depth of the earthquakes. Figure 2 (Attachment 02.05.02-03B) shows a histogram of focal depths for the events shown in Figure 2.5-294 that have a 68% confidence vertical error ellipsoid projection of 5 km or less, and were recorded by at least one station within 20 km of the epicenter. These events represent the best-constrained hypocenter locations, and should have minimum bias in the focal depth estimates due to uncertainty in the assumed velocity model. Therefore these events are the most appropriate subset to use in judging the depth distribution of earthquakes.

Figure 2 (Attachment 02.05.02-03B) shows that only one of the 19 well-constrained events has an estimated focal depth less than 4 km and that the remaining 18 focal depth estimates are between 5 and 22 km. This distribution derived for events in the vicinity of the Bellefonte site is consistent with results for the eastern Tennessee seismic zone as a whole (FSAR Subsection 2.5.7, Reference 292), showing 90% of the focal depth estimates below 5 km, with a median depth of 16.8 km, in the mid-crust. The crystalline basement within 25 miles of the site is at a depth of approximately 2 to 2.5 km (see FSAR Figure 2.5-220), so the earthquake hypocenters demonstrate that the seismicity shown in FSAR Figure 2.5-294 is almost exclusively within the crystalline basement. This observation supports the conclusion of the FSAR (see FSAR Subsection 2.5.2.3) that faults shown in FSAR Figure 2.5-294 are not associated with seismicity.

References:

1. Dunn, M.M., and Chapman, M.C., 2006, Fault orientation in the eastern Tennessee seismic zone; a study using the double-difference earthquake location algorithm: Seismological Research Letters, v. 77, p. 494-504.
2. Lahr, J. C., 1989, HYPOELLIPSE/Version 2.0: A computer program for determining local earthquakes hypocentral parameters, magnitude, and first-motion pattern, U.S. Geological Survey Open-File Report 89-116, 92 p.
3. NEIC, 2008, NEIC Monthly Earthquake Data Report file for event 20030429 085939, US Geological Survey. Available at: ftp://hazards.cr.usgs.gov/edr/mchedr/, accessed on 09/25/2008.
4. SEUS SNB, 1981-2006, Southeastern United States Seismic Network Bulletins, Virginia Tech Seismological Observatory. Available at: http://www.geol.vt.edu/outreach/vtso/anonftp/catalog/, accessed on 10/01/2008.
5. Withers, M.M., Horton, S.P., Powell, C.A., Bodin, P.A., Munsey, J.W., and Herrmann, R.B., 2004, Preliminary analysis of aftershocks of the April 29, 2003 4.6 M (sub W) Fort Payne, Alabama, earthquake: Seismological Research Letters, v. 75, abstracts of 75th annual ES-SSA, p. 445.

6. Bollinger, G.A., M.C. Chapman and T.P. Moore (1979). Central Virginia Regional Seismic network: Crustal Velocity Structure in Central and Southwestern Virginia, NUREG/CR-1217, Division of Reactor Safety Research, U.S. Nuclear Regulatory Commission, Washington, D.C., 187 p.

This response is PLANT-SPECIFIC.

ASSOCIATED BLN COL APPLICATION REVISIONS:

No COLA revisions have been identified associated with this response.

ASSOCIATED ATTACHMENTS/ENCLOSURES:

Attachment 02.05.02-03A

Attachment 02.05.02-03B

Attachment 02.05.02-03C

NRC Letter Dated: September 19, 2008

NRC Review of Final Safety Analysis Report

NRC RAI NUMBER: 02.05.02-04

Please describe in detail any differences between the NMSZ source modeling used for the Bellefonte COLA and the Clinton ESP application.

BLN RAI ID: 1834

BLN RESPONSE:

There are two differences between the Bellefonte COLA (BLN) model for New Madrid (NM) and the final Clinton ESP application model (Appendix B to FSAR Subsection 2.5.7, Reference 294) for NM. The first difference is in the estimate of the earthquake cluster recurrence rates for the Brownian Passage Time (BPT) recurrence model, and the second is the implementation of the New Madrid earthquake cluster (BPT) recurrence model.

The BLN earthquake cluster recurrence rates were calculated based on a simulation of dates for prehistoric events performed in a 2003 NM analysis as described in FSAR Subsection 2.5.2.4.4.1.3. The simulated dates were based on data from primarily the Northeast quadrant of the NM region. The BPT rates were based on a t_0 of January 1, 2003 and a 50-year exposure time. FSAR Table 2.5-215, "Earthquake Frequencies for Repeating Large Magnitude Earthquakes," lists the resulting rates.

The final set of Clinton ESP application rates were computed in November 2005. At that time separate simulations of dates for the NE, central, and SW portions of the New Madrid region were developed. The sets of sites for each simulation were slightly different than those used for Bellefonte. The sets of simulated dates to estimate the rates were combined. A t_0 of October 31, 2005, was used along with a 60 year exposure time for the BPT rates. The attached Table 1 (Attachment 02.05.02-04A), which is Table 4.1-3 from the Appendix B of the EGC ESP (Clinton ESP) application, lists the resulting rates. BLN FSAR Table 2.5-215 (Sheet 1 of 7) lists the resulting rates for the Bellefonte site.

The net effect is that the simulated set of dates used for Bellefonte produced a 1.1% higher average Poisson rate than the combined set of simulated dates used for the Clinton ESP. The average Poisson real time rates for Bellefonte are 0.2% lower than those for Clinton, as the difference in BPT rates between Bellefonte and the Clinton ESP application in Table 2 below show.

Table 2 - Mean annual rate of NM (clustered) earthquakes

	Bellefonte	Clinton
Poisson	0.002760	0.002731
BPT	0.001242	0.001245
Average	0.002001	0.001988

The second difference is in the implementation of the New Madrid earthquake cluster (BPT) recurrence model. The Clinton ESP model used two models for magnitude values occurring during earthquake clusters in NM. Model A was given a weight of 2/3, and used magnitudes that were similar in size to the 1811-1812 NM sequence. Model B was given a weight of 1/3 and had three possible sequences: one-third of ruptures are the same as Model A, one-third of sequences contain a smaller rupture of the New Madrid North fault, and one-third of the sequences contain a smaller rupture of the New Madrid South fault. The difference in magnitude of these smaller ruptures from the 1811-1812 ruptures was set to be no

more than one-half magnitude unit, and no magnitude was less than **M**7. In implementation of this model for the Bellefonte site, the following simplifying assumption was used: Model A was assigned a weight of

1.0, and Model B was assigned a weight of 0.0. This is slightly conservative because it assumes that all magnitudes are similar in size to the 1811-1812 NM sequence and ignores the possibility of smaller magnitudes during some (but not all) of the sequences.

This response is PLANT-SPECIFIC.

ASSOCIATED BLN COL APPLICATION REVISIONS:

No COLA revisions have been associated with this response.

ASSOCIATED ATTACHMENTS/ENCLOSURES:

Attachment 02.05.02-04A

NRC Letter Dated: September 19, 2008

NRC Review of Final Safety Analysis Report

NRC RAI NUMBER: 02.05.02-05

FSAR Section 2.5.2.4.4.1.3 of the Bellefonte FSAR states that a time-dependent equivalent Poisson rate for large repeating earthquakes may be obtained given the "present time (t0) measured from the date of the most recent event." The equivalent Poisson rate is computed from the time-dependent renewal probability according to Equation 2.5.2-9. The computation of t0 requires an assumption about the present time.

What "present time" was used when estimating t0 for the NMSZ mainshocks and should the "present time" really be time of first commercial power generation? Additionally, you assumed a power plant life-span of 50 years, but increasing this to 60 years might be reasonable. Please show the effect of a joint increase of t0 and Δt on the NMSZ event rates and 10^{-4} probabilistic hazard at the Bellefonte Units 3 and 4 site.

BLN RAI ID: 1835

BLN RESPONSE:

The present time (T_o) used for the New Madrid Seismic Zones (NMSZ) calculation for the Clinton ESP was November 1, 2005 and for Bellefonte COL was January 1, 2003. These "present times" represent the dates the evaluations (calculations) were performed for each application and not the time of first commercial power generation.

While 60 years may be a reasonable design life span for a power plant, the license will only be granted for 40 years. Hence the exposure time (Δt) used in the Bellefonte FSAR is 50 years, which assumes a 40-year license plus 10 years for licensing and construction.

Table 1 contains calculations of the occurrence rate for New Madrid earthquake sequences using three different assumptions (models) of T_o and Δt for Bellefonte Units 3 & 4. Model A represents the present time (T_o) and exposure time (Δt) used in the Bellefonte FSAR. Models B and C include different assumptions of T_o and Δt to assess their effect on NMSZ earthquake rates. The results from two recurrence methods, Poisson and Brownian Passage Time (BPT), are weighted equally to obtain the mean rate.

Table 1 Recurrence Rates for Bellefonte, Units 3 & 4.

Model	Present Time (T_o)	Exposure Time (Δt)	Mean Poisson Rate	Mean BPT rate	Mean Rate
A	1/1/03	50 yrs	0.002760	0.001242	0.002001
B	10/1/08	50 yrs	0.002746	0.001297	0.002021
C	10/1/18	40 yrs	0.002724	0.001337	0.002031

Model A uses a T_o of January 1, 2003, and a 50-year exposure time. Model B assumes a T_o of October 1, 2008, and a 50-year exposure time. Model C assumes that it takes 10 years to license and build BLN Units 3&4 and *no* large earthquake occurs at New Madrid in the next 10 years. For Model C, T_o is set to

October 1, 2018, and a 40-year exposure time is used. Results are presented in Table 1 for Poisson, BPT, and mean occurrence rates.

The variation in the rates among the modes is only a few percent. As T_0 moves to a later date, the Poisson rates decrease slightly (longer open interval since the 1811-1812 sequence) and the Brownian Passage Time (BPT) rates increase slightly. This results in a slight increase in the mean rate (Table 1).

Given the relationship between earthquake rate and hazard, whereby the frequency of exceedence of ground motion amplitudes is proportional to the earthquake rate, an increase of a few percent in earthquake rate will result in a similar small increase in frequency of exceedence of ground motion amplitudes, particularly since the NMSZ contributes only a fraction of the total hazard at the site. We continue to believe that Model A is the appropriate model given the original analysis that was conducted in 2003 for the Clinton plant. The alternative models give occurrence rates that are within 1.5% of the Model A rate, and the effect on total seismic hazard would be less that 1.5% because the New Madrid seismic zone does not contribute all of the hazard at the Bellefonte site. This achieves consistency of models across sites, and does not project times in the future at which plants might be constructed. For these reasons, the plant seismic design has not been changed by the effects of the alternative models.

This response is PLANT-SPECIFIC.

ASSOCIATED BLN COL APPLICATION REVISIONS:

No COLA revisions have been associated with this response.

ATTACHMENTS/ENCLOSURES:

None

NRC Letter Dated: September 19, 2008

NRC Review of Final Safety Analysis Report

NRC RAI NUMBER: 02.05.02-06

FSAR 2.5.2.4.4.5 explains the deaggregation of hazard for the determination of controlling earthquakes. FSAR Figures 2.5-281 and 2.5 - 283 show the contribution from **M**5 to **M**5.5 earthquakes at distances of 0 to 20 km with deaggregated epsilon (ε) values. Please explain the relative variability of ε values for the M and R bins in these two figures and, specifically, if the low ε values in Figure 2.5 -281 imply that the probabilistic 1E-4 ground motion is primarily associated with ground motions that are smaller than the median motion for the M and R bin at 5-10 Hz, as well as the impact of the low ε values to the GMRS at frequencies greater than 5 Hz.

BLN RAI ID: 1836

BLN RESPONSE:

FSAR Figure 2.5-281 shows the deaggregation of seismic hazard for high frequencies (5 and 10 Hz) at ground motions corresponding to a mean annual frequency of exceedence of 1E-4. The contribution from values of ε below zero indicates that most local earthquakes of $5 \leq \mathbf{M} \leq 6$, if they occur within about 20 km of the site, will cause high-frequency ground motions above the 1E-4 amplitudes. These earthquakes comprise about one-half of the hazard for these ground motion amplitudes. The remaining hazard comes from large earthquakes ($\mathbf{M} \simeq 7.5$) in the New Madrid seismic zone, which is about $R \simeq 360$ km from the site. FSAR Figure 2.5-281 indicates that these earthquakes contribute to hazard at the high-frequency, 1E-4 amplitudes, but only if their ground motion amplitudes lie above the median amplitudes for that **M** and R. This will occur, of course, for one-half of these earthquakes.

By comparison, FSAR Figure 2.5-283 shows the deaggregation of seismic hazard for high frequencies at ground motions corresponding to a mean annual frequency of exceedence of 1E-5. These are higher amplitudes of ground motion, and Figure 2.5-283 shows that only about one-half of local earthquakes (**M** 5 to 6, $R \leq 20$ km) will cause ground motions exceeding the 1E-5 amplitudes. These local earthquakes comprise about 85% of the total hazard of 1E-5.

The seismic hazard analysis accounts for aleatory uncertainty in ground motions, and the 1E-4 and 1E-5 amplitudes have been calculated accounting for this distribution. Thus the 1E-4 and 1E-5 uniform hazard response spectra (UHRS), and the ground motion response spectra (GMRS) derived from those spectra, take into account the range of ε values that may occur during each earthquake. The 1E-4 amplitudes, for example, account for the fact that most local earthquakes with $5 \leq \mathbf{M} \leq 6$ will exceed those amplitudes, and that one-half of the $\mathbf{M} \simeq 7.5$, $R \simeq 360$ km earthquakes will exceed those amplitudes.

The Regulatory Guide 1.208 procedure for establishing controlling earthquake magnitudes and distances, which was followed as discussed in FSAR Subsection 2.5.2, is a convenient, approximate procedure to account for different earthquakes contributing to high- and low-frequency ground motion hazards. The controlling magnitudes and distances are used to scale spectral shapes between the spectral frequencies at which hazard calculations have been performed. Because the aleatory uncertainties in ground motion equations are similar at 5 Hz, 10 Hz, 25 Hz, and 100 Hz, adjusting the spectral shape to account for different ε values will not have a significant effect, especially once these shapes are anchored to the UHRS amplitudes at 5 Hz, 10 Hz, 25 Hz, and 100 Hz. Thus, the low ε have no appreciable impact on the GMRS.

This response is PLANT-SPECIFIC.

ASSOCIATED BLN COL APPLICATION REVISIONS:

No COLA revisions have been associated with this response.

ASSOCIATED ATTACHMENTS/ENCLOSURES:

None

NRC Letter Dated: September 19, 2008

NRC Review of Final Safety Analysis Report

NRC RAI NUMBER: 02.05.02-07

FSAR Section 2.5.2.4.4.4 states that CAV filter is used in seismic hazard calculation. Please provide in detail how you applied the CAV filter to the Bellefonte site-specific seismic hazard calculation.

BLN RAI ID: 1837

BLN RESPONSE:

The CAV filter was applied to the Bellefonte seismic hazard calculation following the equations of Reference 394 of FSAR Subsection 2.5.7. Specifically, the probability that a ground motion is damaging is given by their Eqn. (2-7):

$$P(CAV>0.16g\text{-}s|PGA,M,V_{S30}) = 1 - \Phi(\varepsilon^*_{CAV}) \quad \text{for } PGA \geq 0.025g \qquad (1)$$
$$= 0 \quad \text{for } PGA < 0.025g$$

where 0.16g-s is the CAV threshold at which ground motions are considered to be damaging, PGA is peak ground acceleration, M is magnitude, and V_{S30} is shear-wave velocity in the top 30 m. In Eqn. (1), Φ is the cumulative distribution function of the normal distribution, and ε^*_{cav} is the number of standard deviations that ln(0.16g-s) is above or below the predicted ln(CAV) value for that earthquake. The median value of ln(CAV) is given by Eqn. 2-2 of Reference 1, and the standard deviation of ln(CAV) is given by their equation in Table 2-3, using the duration calculated by their Eqn. 2-4 (FSAR Subsection 2.5.7, Reference 394). From the median and standard deviation of ln(CAV), ε^*_{cav} is calculated as

$$\varepsilon^*_{CAV} = [\ln(0.16) - \text{median}(\ln(CAV))]/\sigma_{\ln CAV} \qquad (2)$$

which is a simplified version of their Eqn. 2-8.

The standard hazard integral for PGA can be written in the form

$$\nu(Sa>z) = \Sigma(n(M>M_{min})\iint f_m(M)\, f_r(R)\, P[PGA>z \mid M,R]\, dR\, dM \qquad (3)$$

The CAV filter is applied within the hazard integral, as described in Section 4 of Reference 1. For PGA, this involves replacing the quantity P[PGA>z|M,R] in the standard hazard integral with the quantity $P[PGA > z \wedge CAV > 0.16gs|\, M,R,V_{S30}]$. This quantity represents a double integral over ε_{PGA} and ε_{CAV} (the symbol $\wedge$ indicates "and"), where ε_{PGA} is the difference between the actual ln[PGA] and the median amplitude predicted by the attenuation equation for magnitude M and distance R, normalized by the standard deviation of ln[PGA].

For spectral acceleration, one must recognize that CAV depends on PGA (and, therefore, on ε_{PGA}) and that ε_{Sa} is correlated with ε_{PGA}. As a consequence, the quantity $P[Sa > z \wedge CAV > 0.16gs|\, M,R,V_{S30}]$ represents a triple integral over ε_{Sa} ε_{PGA}, and ε_{CAV}. FSAR Reference 394 provides values for the correlation coefficient between PGA and Sa at various periods.

Because CAV depends on the PGA experienced by the structure, not on the PGA at bedrock, the PGA and the Sa in the equations above include site-response effects.

In summary, the hazard calculations with the CAV filter considers the possible combinations of magnitude and distance, but counts only those earthquakes with combinations of ε values such PGA> z (or Sa> z, as appropriate) *and* CAV>0.16g-s.

This response is PLANT-SPECIFIC.

ASSOCIATED BLN COL APPLICATION REVISIONS:

No COLA revisions have been associated with this response.

ASSOCIATED ATTACHMENTS/ENCLOSURES:

None

NRC Letter Dated: September 19, 2008

NRC Review of Final Safety Analysis Report

NRC RAI NUMBER: 02.05.02-08

FSAR Section 2.5.2.2.1 briefly covered the EPRI SOG's seismic source characterization related to the Bellefonte Units 3 and 4 site. The Dames and Moore team assigned lower probabilities of activity to Source Zones 41 and 53. Please justify how the Dames and Moore source model for these two zones adequately characterizes the seismic hazard for the Bellefonte site and the overall impact of the low probability of activity on the final hazard curves for the site.

BLN RAI ID: 1838

BLN RESPONSE:

The Bellefonte site lies within Dames & Moore Source 04, very close to the boundary of Dames & Moore Source 4A. These two sources dominate the hazard for the Dames & Moore interpretations. Dames & Moore Sources 41 and 53 lie to the southeast of the site. The closest approach of Source 41 is roughly 110 km from the site, and the closest approach of Source 53 is roughly 210 km from the site. These two sources are default sources for Triassic Basins on the east coast, and are considered active for the case in which the Triassic Basins are not the correct source of earthquakes with $m_b>5$.

The EPRI-SOG seismic source characterization comprises interpretations and evaluations from six earth science teams (ESTs). As such, the Dames & Moore interpretation is one of six EST interpretations of the causes of earthquakes in the eastern US with $m_b>5$. As one interpretation of six, it is a reasonable that earthquakes with $m_b>5$ may be associated with Triassic Basins (with some probability), or alternatively that they may occur in a background zone (with some probability). Stated another way, Dames & Moore Source 41 has a probability of not being active of 0.88 (see FSAR Table 2.5-208B), and this is one interpretation out of six. Considering the entire EPRI-SOG model with the different interpretations of the six ESTs, it is reasonable that there is a large region of the eastern US Piedmont physiographic province (i.e., Dames & Moore Source 41) that will never produce earthquakes with $m_b>5$ in the current crustal stress regime, with probability 0.147 (0.88 divided by 6 since the interpretations of the 6 ESTs are equally weighted). The alternative is to assume that earthquakes with $m_b>5$ will occur, with certainty, at every location within the Piedmont, at some time in the future. Viewed in light of the fact that the Dames & Moore interpretation is simply one of 6 interpretations, the Dames & Moore interpretation for Source 41 is reasonable. The same analysis and argument applies to Source 53.

In any case, the distances of Dames & Moore Sources 41 and 53 from the site, and the dominance of Dames & Moore Sources 4 and 4A on the hazard, mean that modifying the probabilities of activity of Dames & Moore Sources 41 and 53 to some alternative value will have very little impact on the final hazard curves for the site.

This response is PLANT-SPECIFIC.

ASSOCIATED BLN COL APPLICATION REVISIONS:
No COLA revisions have been associated with this response.

ASSOCIATED ATTACHMENTS/ENCLOSURES:

None

Attachment 02.05.02-02A

(2 pages including cover sheet)

Figure 1

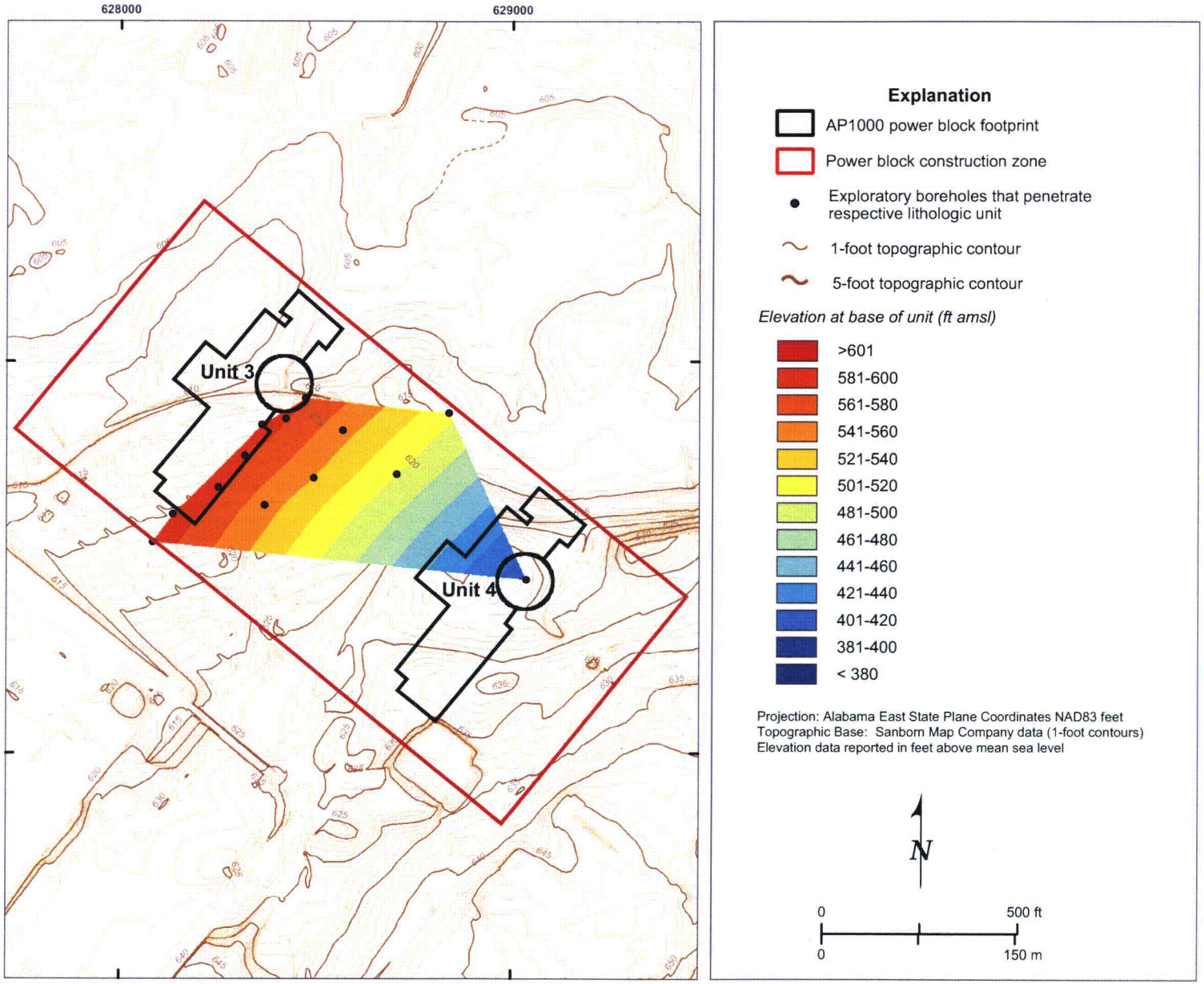

FIGURE 1
Elevation of the Base of Layer C in Map View (from FSAR Figure 2.5-297)

Attachment 02.05.02-02B

(2 pages including cover sheet)

Figure 2

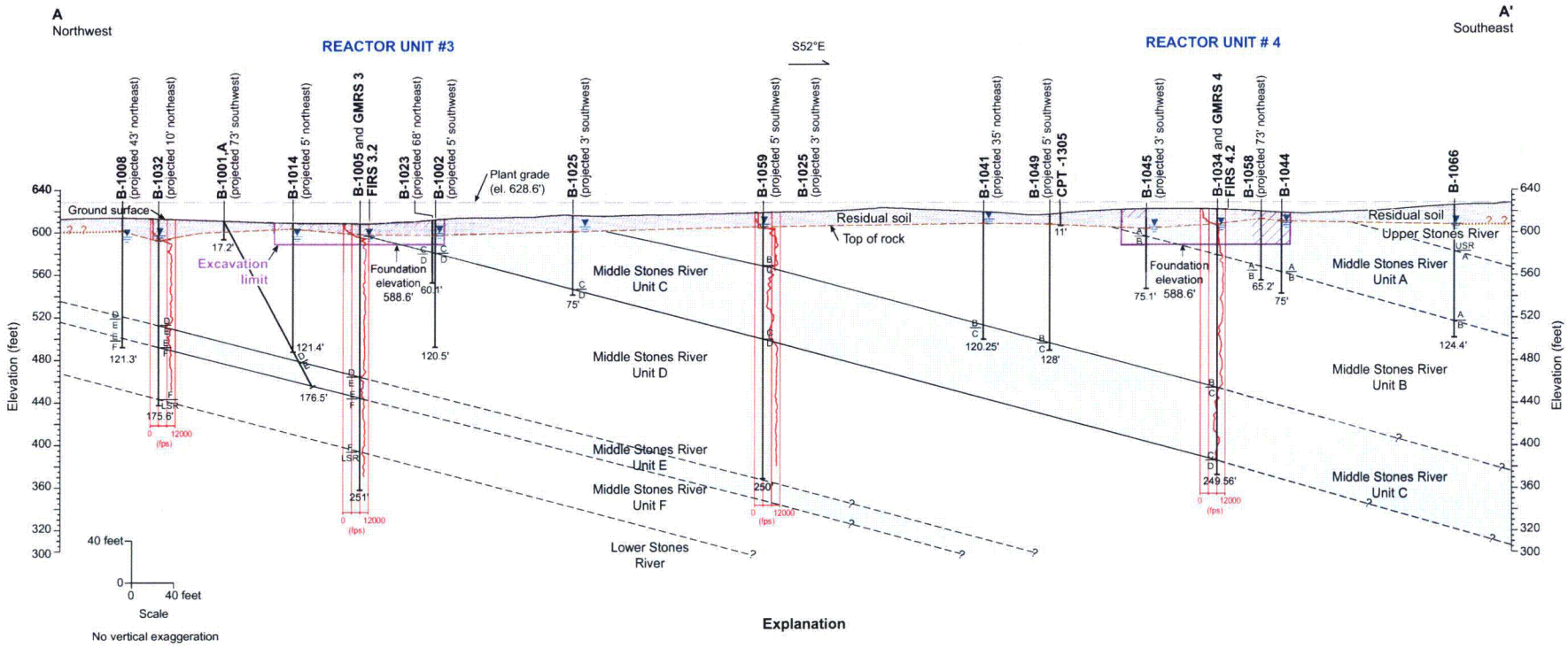

Explanation

Symbols

- Observed water level (during drilling)
- Lithologic contact
- Geologic contact, dashed where approximate
- Rock/soil interface, thin dashed line where extrapolated, dotted where approximate
- Measured shear wave velocity (Vs)

Unit Descriptions

Upper Stones River	Limestone and argillaceous limestone
Unit A	Argillaceous and silty limestone*
Unit B	Limestone
Unit C	Argillaceous and silty limestone*
Unit D	Limestone
Unit E	Argillaceous and silty limestone*
Unit F	Limestone
Lower Stones River	Limestone and argillaceous limestone

Note: Lithology is interpolated between borings that lie within 10 feet of the section line. Contacts in more distant borings are shown for information purposes. The Stones River Group is comprised of Upper Stones River, Middle Stones River, and Lower Stones River.

*Argillaceous and silty limestone is described as "Shale with limestone interbeds" in field descriptions on boring logs.

FIGURE 2
Cross Section, Bellefonte Nuclear Plant, Unit 3 (from FSAR Figure 2.5-339)

Attachment 02.05.02-02C

(2 pages including cover sheet)

Figure 3

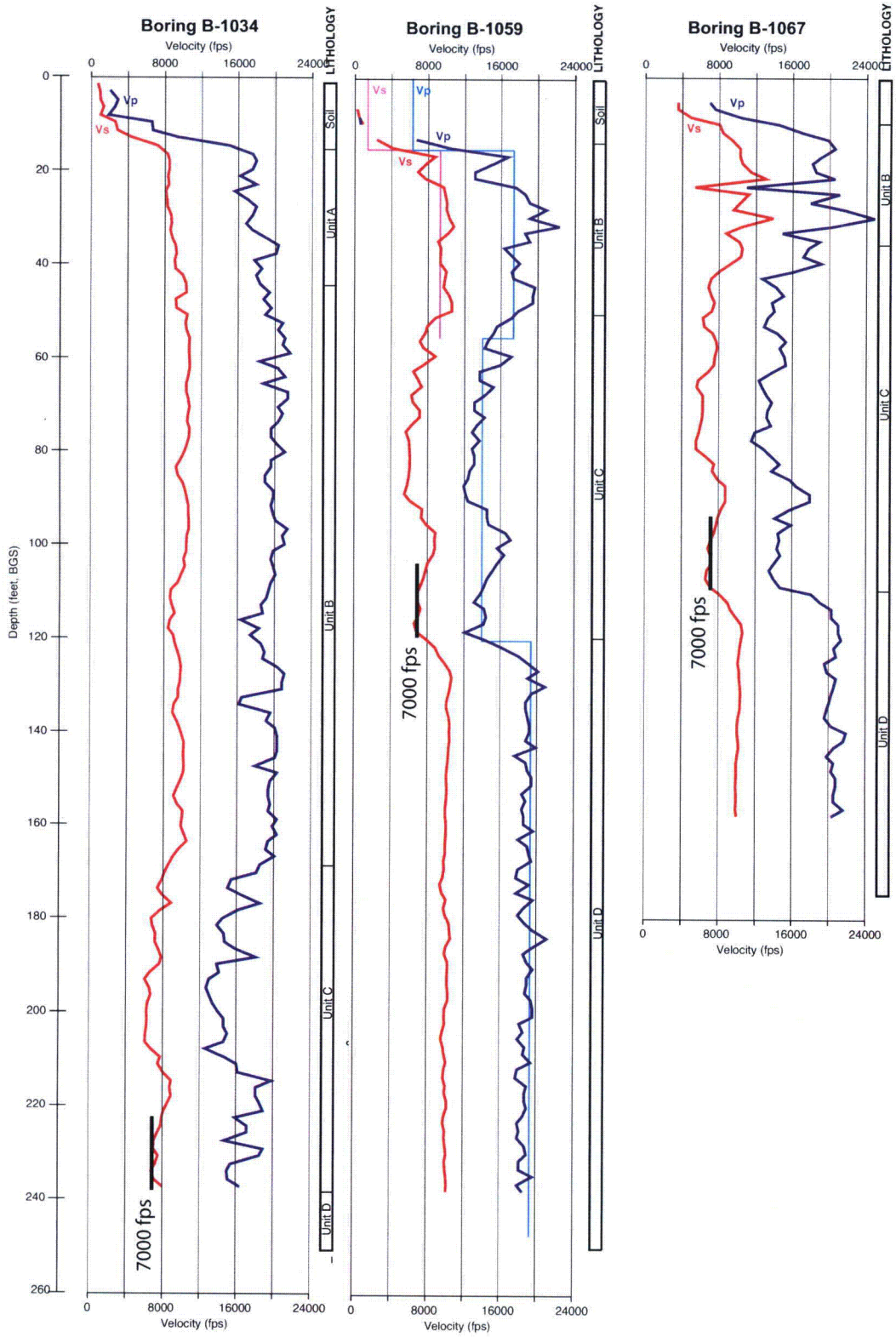

FIGURE 3

Velocity Logs Intersecting Layer C (from FSAR Figures 2.5-334, 2.5-336, and 2.5-338)

Attachment 02.05.02-02D

(2 pages including cover sheet)

Figure 4

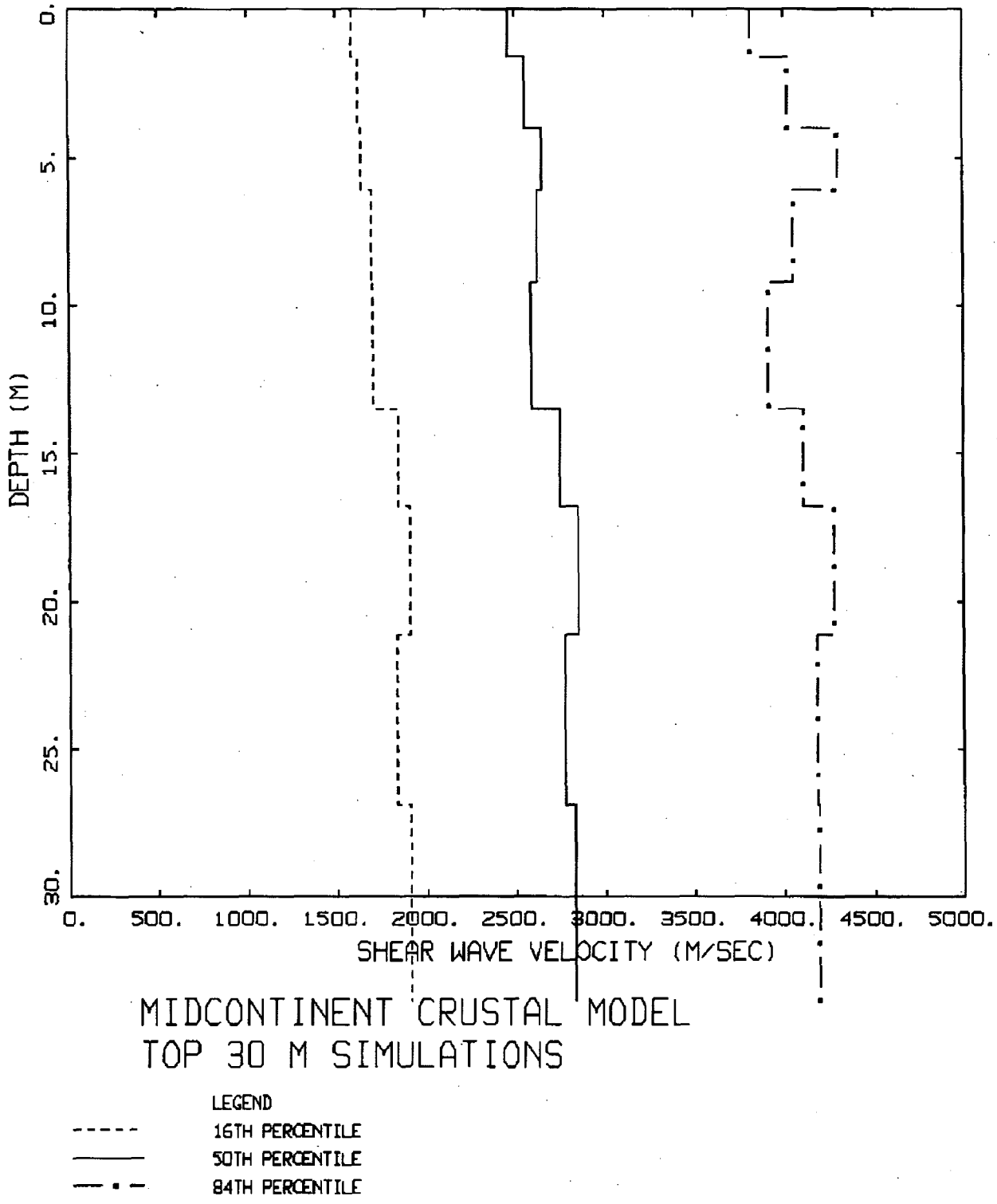

FIGURE 4

Median and ± 1σ Shallow Shear-Wave Velocities Based on Randomizing About the EPRI (1993, 2004) Base-Case of 2.84 km/sec Using an Empirical Correlation Model (EPRI, 1993)

Attachment 02.05.02-02E

(2 pages including cover sheet)

Figure 5

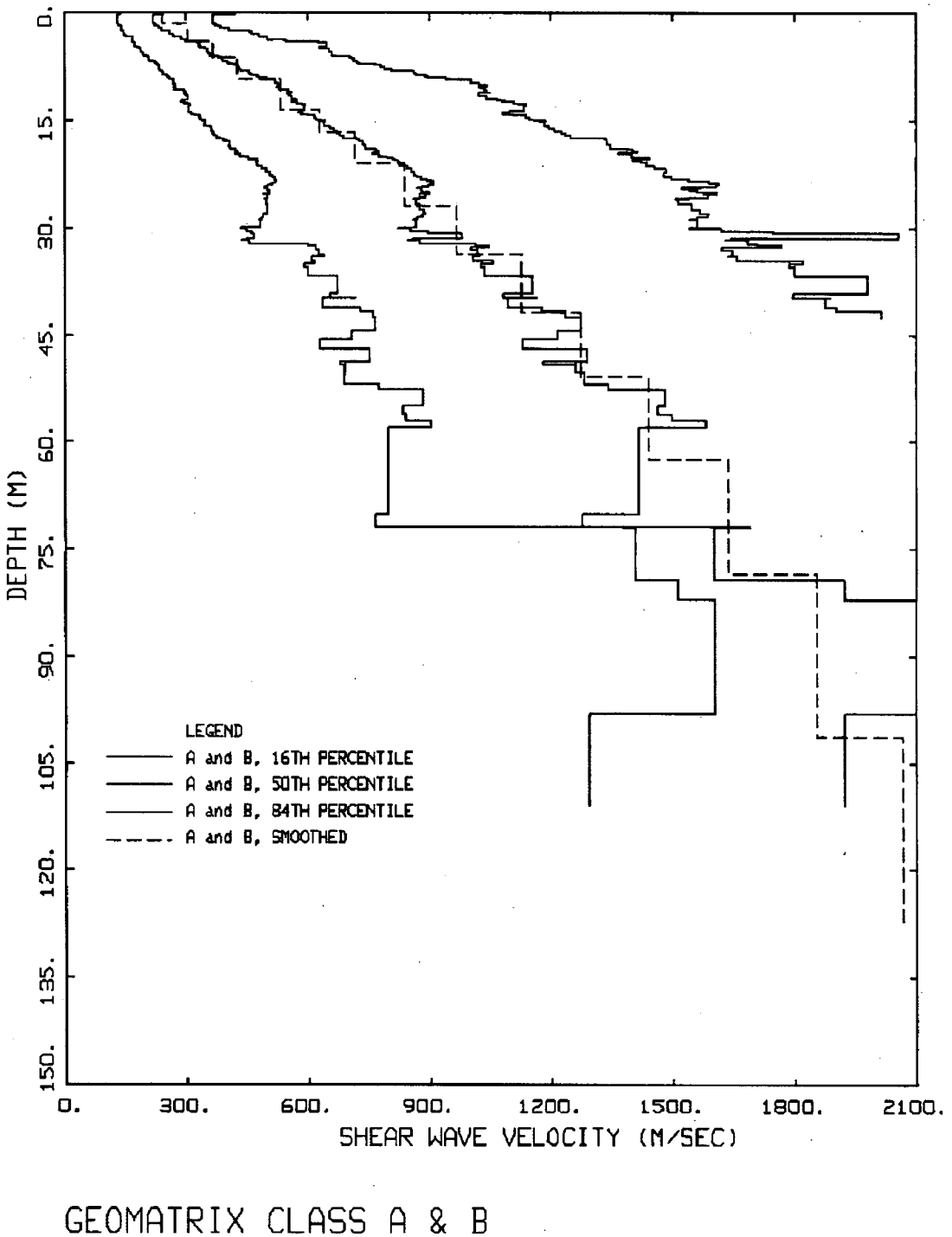

FIGURE 5
Median and ± 1σ Shallow Shear-Wave Velocities from Measured Profiles at Soft Rock Sites in WNA (Geomatrix Site Categories A and B)

Attachment 02.05.02-03A

(2 pages including cover sheet)

Figure 1

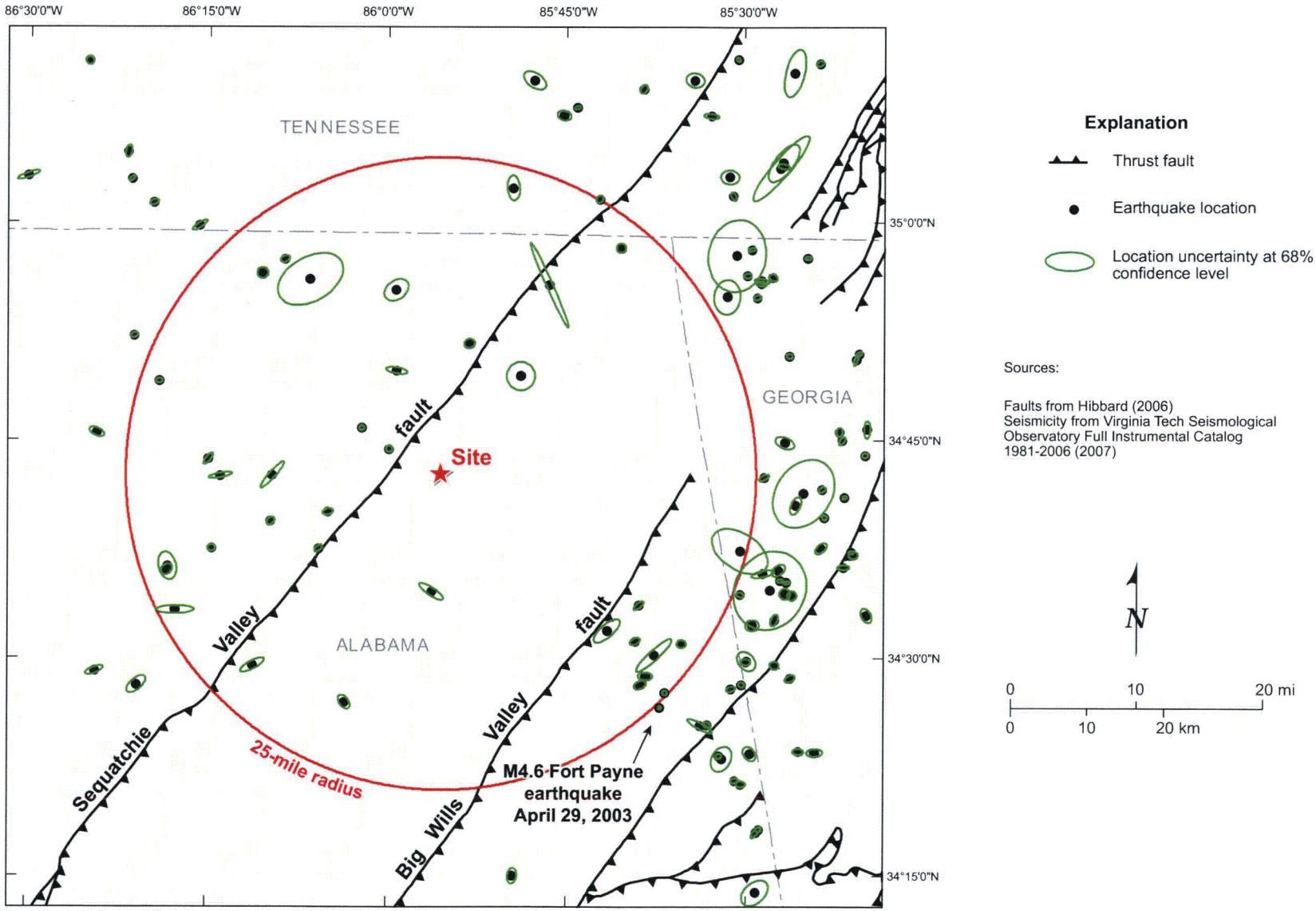

(Reference 408 and 407)

FIGURE 1
Location Uncertainty of Seismicity

Attachment 02.05.02-03B

(2 pages including cover sheet)

Figure 2

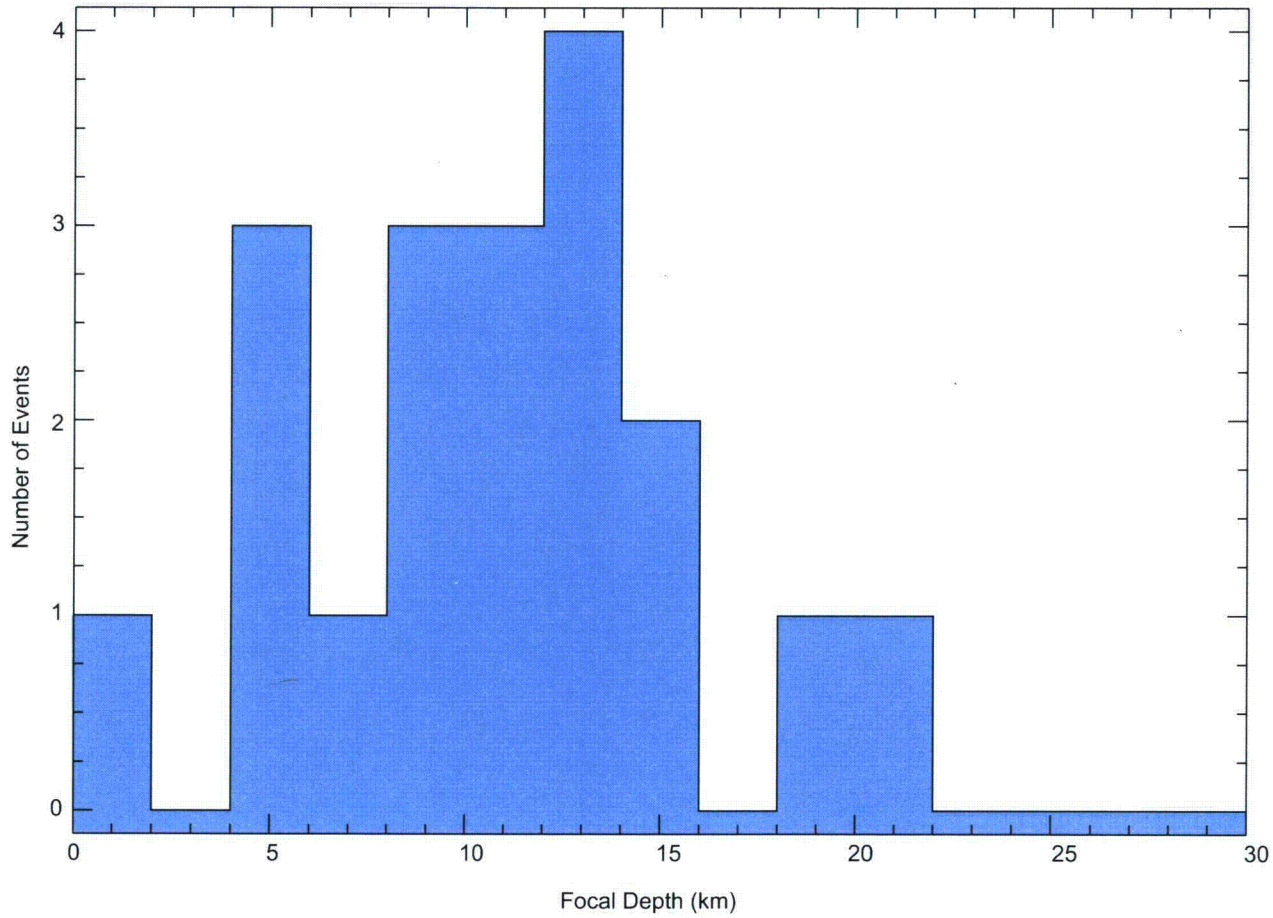

FIGURE 2
Histogram of focal depths for hypocenter locations with ERZ less than 5km and with minimum station distance less than 20 km

Attachment 02.05.02-2A
TVA letter dated October 20, 2008
RAI Responses

Attachment 02.05.02-03C

(5 pages including cover sheet)

Table 1 - Earthquake Data from FSAR Figure 2.5-294

Table 1 - Earthquake Data from FSAR Figure 2.5-294

Date	Time	Lat.	Lon.	Depth (km)	Const.	mblg	mdur	ERHMAX (km)	AZ	ERHMIN (km)	ERZ (km)
9/28/1981	18:3:35.1	34.573	-85.435	8.6			2.1	0.6	360	0.6	1.1
12/23/1981	16:10:12.2	34.825	-85.813	6.3			1.6	1.8	360	1.8	1.4
1/2/1981	2:0:26.3	35.184	-86.417	11.3			2	0.5	360	0.5	1.2
2/23/1982	9:19:8.8	34.575	-85.445	6.5			2.3	0.7	360	0.7	1.5
11/23/1982	4:51:0.1	35.068	-85.446	0			2	2.9	-52	1.2	
1/8/1983	22:30:37.2	34.915	-85.526	0			2.3	2.2	-85	1.7	
1/31/1983	23:4:8.6	34.962	-85.512	0			2.1	4.6	-80	3.7	
2/27/1984	17:8:11	34.662	-85.39	10.9			2.1	0.3	360	0.3	0.4
8/9/1984	2:42:35.2	34.602	-86.304	15.4			2.9	0.8	-43	0.6	1.6
8/9/1984	7:35:7.8	34.606	-86.303	8.6			1	1.8	76	1.1	2.7
8/26/1984	8:16:26.5	34.765	-86.035	7.6			1.3	0.3	360	0.3	0.7
2/5/1985	8:49:39	34.942	-86.174	9.6			0.9	0.7	360	0.7	0.6
2/19/1985	14:2:50	34.971	-85.674	7			1.1	0.6	360	0.6	1.5
4/11/1986	6:5:25.9	34.676	-85.43	13	Y		0	1.2	-65	0.6	0.8
4/19/1986	7:40:53	35.187	-85.51	27.3			3	0.3	50	0.2	0.8
8/29/1986	7:44:38.4	34.302	-85.486	18.7	Y		1.5	0.9	-48	0.3	
8/29/1986	7:49:3.5	34.389	-85.538	10.3			1.5	0.4	-16	0.3	0.5
9/3/1986	17:35:48.3	34.741	-85.997	17.1			1.8	0.4	81	0.4	
2/3/1987	10:32:36.4	34.818	-86.316	9.6			2.4	0.4	-11	0.3	1
2/24/1987	9:58:10.6	34.733	-85.333	9.9	Y		2.4	0.4	-9	0.3	0.7
6/9/1987	20:20:55	34.55	-85.332	9.8	Y		0	1	61	0.6	1.2
11/8/1987	5:15:7.2	34.76	-85.369	9.5	Y		0.5	0.6	-84	0.4	1.1
1/10/1988	13:53:13.2	34.579	-85.466	10.1	Y		0.3	5.2	-58	4.5	2.3
3/6/1988	7:6:28.6	34.305	-85.482	13.8	Y		1.4	0.4	-12	0.3	0.5
4/26/1988	0:18:0.1	35.022	-86.325	11			2	0.6	-22	0.3	0.9
6/16/1988	9:0:44.4	34.497	-85.5	11.9	Y		1.2	0.6	6	0.4	0.3
10/13/1988	9:17:26	34.357	-85.507	13.1			2.1	0.6	0	0.4	0.6
2/20/1989	8:45:48.7	34.759	-86.403	17.9			1.3	1	25	0.5	2.5
5/8/1989	2:8:53.9	34.393	-85.404	9.2			1.4	1	-3	0.5	1
6/11/1989	4:19:50.2	34.831	-85.987	22.4			0.8	1.4	10	0.4	10.3
7/1/1989	4:41:14.5	34.478	-85.438	14.7	Y		2.3	0.7	-24	0.4	0.6
8/12/1989	1:57:16.4	34.669	-86.082	7.7			1.6	0.7	-14	0.4	1.6
10/16/1989	2:7:36.5	34.386	-85.534	11.8			1.6	1.7	-60	1.2	1.6
12/9/1989	20:24:56.7	34.233	-85.487	10.6			1.4	2	-40	1.3	2

Table 1 (cont) - Earthquake Data from FSAR Figure 2.5-294

Date	Time	Lat.	Lon.	Depth (km)	Const.	mblg	mdur	ERHMAX (km)	AZ	ERHMIN (km)	ERZ (km)
5/4/1990	21:40:37.2	34.466	-85.521	12.4	Y		2.5	0.6	-17	0.3	0.6
6/13/1990	11:1:57.9	34.843	-85.345	10.8	Y		1.8	0.8	-68	0.2	0.9
7/27/1990	5:56:27.4	34.392	-85.495	8.1			2.1	1	53	0.7	1
9/19/1990	21:56:45	34.539	-85.491	0			3	0.9	-3	0.7	1.3
1/21/1991	7:3:23.7	34.486	-86.404	11			1.9	1.2	-22	0.4	1.3
3/28/1991	10:26:16.7	34.627	-86.243	12.7			1.8	0.5	-1	0.4	1
8/17/1991	17:59:9.2	34.914	-85.483	21.4	Y		2.7	0.5	-15	0.3	0.8
10/22/1991	6:30:57.2	34.493	-85.46	8.4			2	0.6	8	0.5	1.1
11/10/1991	9:54:42.1	34.75	-85.365	1.9	Y		1.9	0.6	-51	0.3	1
7/2/1992	3:47:42.7	34.87	-86.351	8.2			2.1	0.5	-20	0.3	0.8
8/8/1992	3:51:41.9	34.588	-85.443	12.9	Y		2	0.4	6	0.2	0.4
12/11/1992	4:39:33.3	34.763	-85.33	7.4			1	1.1	-88	0.4	1.8
12/14/1992	8:55:2	35.122	-85.548	7.4			1.5	1	7	0.3	1.7
6/7/1993	10:35:6	35.03	-85.517	12.6			1.6	0.6	63	0.3	0.9
12/29/1993	2:48:54.4	35.064	-85.446	18.8			1.6	0.8	12	0.3	1.8
4/5/1994	2:33:43.5	34.933	-85.477	11.9			2.3	1	8	0.3	1
4/5/1994	19:47:42.8	34.939	-85.497	4.8			1.9	0.5	-6	0.3	1.4
4/5/1994	22:22:0.4	34.969	-85.491	24.3		3.2	3.4	0.5	-15	0.2	0.4
4/5/1994	23:39:26.8	34.93	-85.478	9.5			1.5	0.7	6	0.3	1.1
5/26/1994	1:57:27.8	34.958	-86.143	8.8			2.3	0.6	-24	0.4	1.2
7/4/1994	7:9:31.5	34.556	-86.292	15.2			0.8	2.4	-1	0.5	
8/29/1994	7:10:17.3	35.062	-85.45	13.9			0.7	5.4	-49	1.1	10.4
9/13/1994	11:3:59.8	34.708	-85.474	5.1	Y		2.6	0.7	-28	0.3	0.9
10/5/1994	23:25:17.5	34.929	-85.774	10.6			1.2	5.9	66	0.4	2.2
5/19/1997	19:45:35.8	34.622	-85.353	2.7		2.9	3.1	0.3	7	0.2	1.2
5/19/1997	22:22:33.9	34.605	-85.364	5.4			1.6	0.8	358	0.3	2.2
8/1/1997	4:48:12.3	34.923	-85.988	0			1.7	1.7	325	1.2	2.3
8/20/1997	16:10:19.8	34.578	-85.937	0			2.3	1.8	33	0.5	4
9/14/1997	7:23:50.5	34.521	-85.654	2.3			1.6	0.7	334	0.4	2.2
9/14/1997	7:24:54.5	34.533	-85.693	8.2			0.8	2.1	319	0.8	6.3
9/14/1997	7:53:37.9	34.505	-85.628	10.7			0.6	3	317	0.6	14.2
10/12/1997	6:55:32.6	34.394	-85.427	0			2	0.7	3	0.4	1.3
10/19/1997	20:45:20.6	34.518	-85.59	1.9			1.7	0.6	2	0.5	2.9
11/3/1997	16:34:59.3	34.471	-85.506	0			2.4	0.4	16	0.3	1.2

Table 1 (cont) - Earthquake Data from FSAR Figure 2.5-294

Date	Time	Lat.	Lon.	Depth (km)	Const.	mblg	mdur	ERHMAX (km)	AZ	ERHMIN (km)	ERZ (km)
1/28/1998	16:44:21.4	34.425	-85.554	0			2.5	0.5	23	0.3	1.8
2/2/1998	7:5:33.1	35.123	-85.754	6.7	Y		1.8	0.9	14	0.6	1.3
2/3/1998	22:18:41.6	34.424	-85.564	0			2.1	1.8	28	0.4	3.2
7/12/1998	22:6:41.7	35.163	-85.795	5	Y		1.7	1.6	34	0.9	1
7/30/1998	10:28:34.7	34.658	-86.161	0			2	0.6	314	0.4	1.5
8/29/1998	3:47:16.5	34.996	-86.262	6.2			1.5	1.1	327	0.3	3.6
10/22/1998	6:52:40.4	34.627	-86.095	0			1.7	0.6	318	0.3	1.8
12/5/1998	5:46:58.5	34.59	-85.452	2.8			2.2	0.4	359	0.2	1.7
2/3/1999	16:13:4.5	35.052	-86.501	9.1			1.9	1.5	340	0.3	4.3
3/9/1999	6:25:43.8	34.959	-85.412	0.6			1.9	0.4	357	0.2	1.1
5/28/1999	12:11:57.9	35.163	-85.571	7.9			1.4	1.2	11	0.9	2.2
9/2/1999	21:48:49.7	35.182	-85.395	15.8			1.7	0.5	341	0.3	1.2
11/12/1999	3:6:33.3	34.849	-85.341	12.1			2.2	0.5	332	0.2	0.6
1/25/2000	20:35:26.4	35.08	86.361	0			2.4	0.8	282	0.4	2.4
3/20/2000	4:54:8	35.049	86.356	8.6			2	0.5	323	0.2	1.4
3/20/2000	10:0:50.2	34.685	-85.362	3.9			2.8	0.3	344	0.2	0.7
3/20/2000	19:36:50.3	34.694	-85.393	3.5			1.7	0.5	331	0.3	1.8
6/21/2000	2:51:20.5	34.627	-85.395	2.9			1.4	0.9	318	0.5	3.3
9/4/2000	2:26:51.8	35.052	-85.522	18.5			1.7	1.2	5	0.9	1
9/9/2000	23:47:27.7	35.132	-85.735	5.5	Y		2.6	0.4	343	0.2	0.6
9/12/2000	10:28:48	35.027	-85.704	3.6			2	0.5	303	0.4	1.1
9/26/2000	1:9:28.9	35.04	-85.824	11.9			0.9	1.6	266	0.8	1.9
1/27/2001	12:8:57	34.748	-85.445	2.4			1.7	1.3	23	0.7	1.5
3/13/2001	2:49:22.2	34.47	-86.345	16.8			1.6	1.5	320	0.7	1.9
3/21/2001	23:35:34.9	34.847	-85.438	0			3.2	0.4	19	0.3	0.7
5/4/2001	1:16:36.4	34.711	-86.159	26.4			1.5	2.2	311	0.4	3.3
6/21/2001	19:37:49	34.862	-85.885	0			2.3	0.7	343	0.6	1.5
8/30/2001	8:33:49	34.545	-85.46	2.4			1.9	0.8	295	0.4	1.4
9/10/2001	17:6:5.2	34.493	-86.185	10.6			1.7	1.7	331	0.5	4.9
10/3/2001	1:44:3.6	34.619	-85.35	5.4			1.9	0.6	357	0.5	2.5
12/8/2001	1:8:22.4	34.71	-86.231	0		3.9	3.7	1.5	349	0.3	1.7

Table 1 (cont) - Earthquake Data from FSAR Figure 2.5-294

Date	Time	Lat.	Lon.	Depth (km)	Const.	mblg	mdur	ERHMAX (km)	AZ	ERHMIN (km)	ERZ (km)
11/27/2002	21:44:43.8	34.598	-85.476	6.9			1.8	1.5	348	0.4	1.8
2/5/2003	1:34:37.1	34.729	-86.248	15.4			1.9	0.9	308	0.3	1.4
4/29/2003	8:59:38.1	34.445	-85.62	9.1		4.6	4.9	0.2	0	0.2	0.4
6/22/2003	23:49:54.2	34.562	-85.649	3.1			1.9	0.8	320	0.3	1.5
7/6/2003	13:59:26.3	34.462	-85.613	1.9			2.5	0.3	41	0.3	1.5
7/15/2003	19:17:14.8	34.481	-85.64	12.3			2.5	0.9	4	0.5	1.3
7/25/2003	7:23:41.1	34.451	-86.058	14.8			2	1	234	0.6	1.1
12/25/2003	1:43:24	34.253	-85.823	7.8			2	1	279	0.6	3.4
3/14/2004	13:39:54.2	34.361	-85.516	9.7			2	0.5	348	0.3	1.8
4/30/2004	2:55:57.9	34.602	-85.454	0			2.4	1	323	0.6	1.9
6/21/2004	9:49:19	34.471	-85.647	6.1			2.2	0.8	335	0.5	3.4
9/20/2004	23:26:18.7	34.69	-85.419	10			2.5	4.7	306	3.5	7.7
11/11/2004	3:28:5.5	34.935	-86.108	8.7			2	4.5	330	2.8	8.2
5/20/2005	14:32:1.6	35.153	-85.643	10.3			1.7	0.6	299	0.4	2.1
9/12/2005	13:20:15.6	34.574	-85.508	16.4			1.7	0.5	21	0.3	0.7
10/16/2005	3:33:42.6	34.498	-85.499	11.2			2.1	1.4	229	1	3
8/7/2006	8:44:27.7	34.937	-85.461	14.2	Y		2.9	0.6	29	0.4	1.2
10/15/2006	18:49:33.5	34.624	-85.508	8			2.2	4	32	2.3	6.5
12/10/2006	5:26:1.5	35.171	-85.43	11			1.1	3.1	284	1.2	7.1

Table 1. Earthquake Data from FSAR Figure 2.5-294.
Column definitions are as follows.
Const: Y if depth is considered well constrained.
mblg: Lg-phase body-wave magnitude.
mdur: duration/coda-length magnitude.
ERHMAX: semi-major, horizontal 68% confidence ellipse axis.
AZ: azimuth of semi-major axis. ERHMIN: semi-minor, horizontal 68% confidence ellipse axis.
ERZ: largest vertical deviation of 68% confidence ellipse from hypocenter.
Blank fields indicates that no value was calculated.

Attachment 02.05.02-04A

(2 pages including cover sheet)

Table 1

(Table 4.1-3 from FSAR Reference 294)

TABLE 4.1-3

EARTHQUAKE FREQUENCIES FOR REPEATING NEW MADRID EARTHQUAKE SEQUENCES

Seismic Hazards Report for the EGC ESP Site

Recurrence Model	Weight	Mean Repeat Time (years)	Equivalent Annual Frequency
Poisson	0.10108	161	6.20E-03
	0.24429	262	3.82E-03
	0.30926	410	2.44E-03
	0.24429	694	1.44E-03
	0.10108	1,563	6.40E-04
Renewal (BPT),	0.10108	333	3.39E-03
$\alpha = 0.3$	0.24429	410	1.07E-03
	0.30926	485	3.02E-04
	0.24429	574	5.95E-05
	0.10108	709	4.30E-06
Renewal (BPT),	0.10108	316	4.85E-03
$\alpha = 0.5$	0.24429	440	2.18E-03
	0.30926	573	8.89E-04
	0.24429	746	2.58E-04
	0.10108	1,032	2.97E-05
Renewal (BPT),	0.10108	325	4.45E-03
$\alpha = 0.7$	0.24429	506	2.25E-03
	0.30926	719	1.02E-03
	0.24429	1,011	3.37E-04
	0.10108	1,521	4.49E-05